

# Light unflavored vector meson spectroscopy around the mass range of 2.4 ~ 3 GeV and possible experimental evidence

Li-Ming Wang<sup>1,3,\*</sup>, Si-Qiang Luo<sup>2,3,4,†</sup> and Xiang Liu<sup>2,3,4,5,‡§</sup>

<sup>1</sup>Key Laboratory for Microstructural Material Physics of Hebei Province,  
School of Science, Yanshan University, Qinhuangdao 066004, China

<sup>2</sup>School of Physical Science and Technology, Lanzhou University, Lanzhou 730000, China

<sup>3</sup>Lanzhou Center for Theoretical Physics, Key Laboratory of Theoretical Physics of Gansu Province  
and Frontiers Science Center for Rare Isotopes, Lanzhou University, Lanzhou 730000, China

<sup>4</sup>Research Center for Hadron and CSR Physics, Lanzhou University and Institute of Modern Physics of CAS, Lanzhou 730000, China

<sup>5</sup>Joint Research Center for Physics, Lanzhou University and Qinghai Normal University, Xining 810000, China

(Dated: February 4, 2022)

In this work, we predict the spectroscopy behavior of these light unflavored vector mesons with masses at the range of 2.4 ~ 3 GeV, which are still missing in the experiment. By presenting their mass spectrum and studying their two-body Okubo-Zweig-Iizuka allowed decay widths, we discuss the possible experimental evidences of these discussed states combining with the present experimental data. Especially, we strongly suggest that our experimental colleagues carry out the exploration of these higher states via the  $e^+e^-$  annihilation into light mesons. It is obvious that BESIII and Belle II will be potential experiments to achieve this target.

## I. INTRODUCTION

As a main body of the hadron family, light hadron spectroscopy has special status in the whole hadron family, which has inspired the classification of hadron based on SU(3) symmetry in 1964 [1, 2], and has aroused the interest from both theorists and experimentalists in exploring exotic states like glueball, hybrid, and multiquark states [3–6]. With the running of BESIII and Belle II, it is a good chance to launch a profound research on light flavor mesons, which can deepen our understanding of how quarks and gluons interact with each other to form hadrons.

Focusing on the study of light unflavored vector meson spectroscopy, we find big progress being made by experiments in the past years [7–9]. A typical example is the observation of the  $Y(2175)$  [10] and the following measurement [11–16] around the  $Y(2175)$ , which have stimulated extensive discussions of decoding the property of the  $Y(2175)$  [17–22]. Among these possible explanations to the  $Y(2175)$ , categorizing the  $Y(2175)$  into the  $\phi$  meson family is a popular one [17, 23, 24], which should still be tested in an experiment. In fact, the light unflavored vector mesons also include these states in the  $\rho$  and  $\omega$  meson families. With the accumulation of data with unprecedented statistical accuracy, a series of  $\rho$  and  $\omega$  states around 2 GeV were observed in experiments [25–33]. By the joint effort from both theorists and experimentalists, our knowledge of light unflavored vector meson spectroscopy below 2.2 GeV has been promoted, which is the situation of the study of unflavored vector meson spectroscopy. But, it is not the whole aspect of light unflavored vector meson spectroscopy.

The experiments have released the data of  $e^+e^-$  annihilation

into light mesons [34–37], where the collision energy reaches up to ~ 3 GeV. When checking these data, we find possible enhancement structures existing in the corresponding invariant mass spectra with mass range from 2.4 GeV to 3 GeV. For example, in the  $e^+e^- \rightarrow \omega\pi^+\pi^-\pi^0$  process [34], several enhancement structures existing in the energy range of 2.4 GeV are obvious. However, in the process of  $e^+e^- \rightarrow \pi^+\pi^-\pi^0$ , we cannot find conspicuous enhancement structure [35]. Thus, we still need more precise data. In the following, we can find many narrow structures above 2.4 MeV in the process of  $e^+e^- \rightarrow K_2^{*0}(1430)K^-\pi^+$  reported by the BaBar Collaboration [36]. The cross section of  $e^+e^- \rightarrow \phi f_2'(1525)$  was also measured by the BaBar Collaboration. Here, there exists possible enhancement clusters around 2.7 GeV and a clear  $J/\psi$  signal [36]. And then, the Belle Collaboration studied the process of  $e^+e^- \rightarrow \phi\pi^+\pi^-$  and  $e^+e^- \rightarrow \phi f_0(980)$  [37], where the event accumulation around 2.4 GeV and 2.6 GeV can be found. We conjecture that these enhancement structures with low significance can be due to these unknown light unflavored vector mesons.

At present, our knowledge of higher states of the light unflavored vector meson family, which have the masses above 2.4 GeV, is obviously absent. This research status causes us to reinforce the investigation of these higher states of the light unflavored vector meson family, which becomes a central task of this work.

In this work, we apply the modified Godfrey-Isgur model [38] to present the masses distribution of the discussed higher states of the light unflavored vector meson family, where their spatial wave functions can be gotten numerically, which can be as the input of the following calculation of their two-body Okubo-Zweig-Iizuka (OZI) allowed decays. For performing the realistic estimate of these OZI allowed decays, the quark pair creation (QPC) model is adopted here [39–41], which was applied to study the strong decay of different kinds of hadrons [23, 42–50]. We hope that our study on mass spectrum and decay width of the  $\rho$ ,  $\omega$ , and  $\phi$  mesons in 2.4 ~ 3 GeV can provide valuable information to the future experimental explorations.

\*Corresponding author

\*Electronic address: [lmwang@ysu.edu.cn](mailto:lmwang@ysu.edu.cn)

†Electronic address: [luosq15@lzu.edu.cn](mailto:luosq15@lzu.edu.cn)

§Electronic address: [xiangliu@lzu.edu.cn](mailto:xiangliu@lzu.edu.cn)

As emphasized in Ref. [51], the BESIII experiment at the BEPCII is still an ideal platform to hunt for light hadrons. We have reason to believe that the present work can attract the BESIII interest of studying this topic in an experiment. In addition, the running of Belle II with the initial state radiation method will be a potential experiment to finding these discussed light unflavored vector mesons.

This paper is organized as follows. After the Introduction in Sec. I, we present the spectroscopy behavior by the modified Godfrey-Isgur (MGI) model and the QPC model, where the mass spectrum and two-body OZI allowed strong decays of these discussed higher states of light unflavored vector meson are given in Sec. II. Finally, the paper ends with a short summary in Sec. IV.

## II. SPECTROSCOPY BEHAVIOR

There were different approaches to study the meson spectroscopy, which include lattice QCD [52, 53], Regge trajectories [44, 54, 55], nonrelativistic potential models [56–58], QCD string approaches [59, 60], relativistic potential models [61, 62], and so on. In this work, we adopt the MGI model [38] by replacing the linear potential with the screened potential in the Godfrey-Isgur (GI) model [63]. Here, the screened potential indicated by the lattice studies [64, 65] was employed in Refs. [66–68], which is also inspired by the the coupled-channel effects [69, 70]. A successful application of the MGI model is to depict the mass spectrum of these observed charmed-strange mesons [38], where the masses of the most observed  $D_s$  mesons can be understood well. Later, the MGI model was further adopted to perform the mass spectrum analysis of charmed mesons [71], charmonia [72, 73], and bottomonia [74]. Along this line, in this work we still apply the MGI model to discuss these higher states of the light unflavored vector meson family. Besides the mass spectrum, the spatial wave functions of these higher unflavored mesons could be extracted for getting the two-body OZI allowed strong decay widths via the QPC model. In Fig. 1, we show the procedure of how to obtain the whole aspect of these higher light unflavored vector meson spectroscopies.

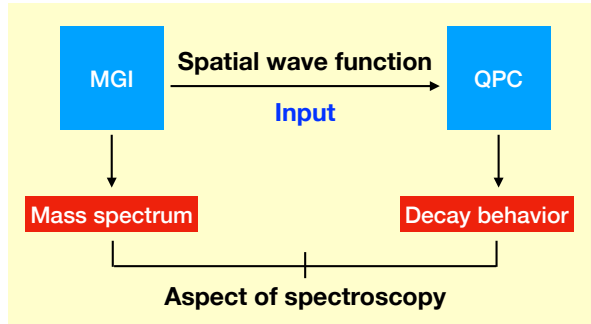


FIG. 1: The procedure of presenting the aspect of light unflavored vector meson spectroscopy.

### A. Mass spectrum

The Hamiltonian depicting the interaction between quark and antiquark in the MGI model is

$$\tilde{H} = \sqrt{m_1^2 + \mathbf{p}^2} + \sqrt{m_2^2 + \mathbf{p}^2} + \tilde{V}_{\text{eff}}(\mathbf{p}, \mathbf{r}), \quad (1)$$

where  $m_1$  and  $m_2$  denote the mass of quark and antiquark, respectively. The effective potential of the  $q\bar{q}$  interaction has the form [38]

$$\tilde{V}_{\text{eff}}(\mathbf{p}, \mathbf{r}) = \tilde{H}^{\text{OGE}} + \tilde{H}^{\text{conf}}, \quad (2)$$

where the first term  $\tilde{H}^{\text{OGE}}$  is a  $\gamma^\mu \otimes \gamma_\mu$  one-gluon-exchange potential, which is a short distance interaction, and the  $\tilde{H}^{\text{conf}}$  in Eq. (2) is a long distance  $1 \otimes 1$  confining interaction. The model includes smearing transformations and momentum-dependent terms. Firstly, the smearing transformations could be expressed as

$$\tilde{V}_{\text{eff}}(\mathbf{p}, \mathbf{r}) = \int d^3\mathbf{r}' \rho_{ij}(\mathbf{r} - \mathbf{r}') V_{\text{eff}}(\mathbf{p}, \mathbf{r}'), \quad (3)$$

where the  $\rho_{ij}(\mathbf{r} - \mathbf{r}')$  is the Gaussian smearing function with

$$\rho_{ij}(\mathbf{r} - \mathbf{r}') = \frac{\sigma_{ij}^3}{\pi^{3/2}} e^{-\sigma_{ij}^2(\mathbf{r}-\mathbf{r}')^2}, \quad (4)$$

$$\sigma_{ij}^2 = \sigma_0^2 \left( \frac{1}{2} + \frac{1}{2} \left( \frac{4m_i m_j}{(m_i + m_j)^2} \right)^4 \right) + s^2 \left( \frac{2m_i m_j}{m_i + m_j} \right)^2. \quad (5)$$

The parameters  $\sigma_0$  and  $s$  in Eq. (5) could be determined by the spin splits of the mesons.

The  $\tilde{H}^{\text{OGE}}$  in Eq. (2) contains Coulomb, contact, tensor, and vector spin-orbit terms, i.e.,

$$\tilde{H}^{\text{OGE}} = \tilde{G}_{12}(r) + \tilde{V}^{\text{cont}}(r) + \tilde{V}^{\text{tens}}(r) + \tilde{V}^{\text{sov}}(r). \quad (6)$$

The Coulomb term  $\tilde{G}_{12}(r)$  is spin independent with definition

$$\begin{aligned} \tilde{G}_{ij}(r) &= \int d^3\mathbf{r}' \rho_{ij}(\mathbf{r} - \mathbf{r}') \left( \sum_k -\frac{4\alpha_k}{3r} \text{erf}(\gamma_k r) \right) \\ &= \sum_k -\frac{4\alpha_k}{3r} \text{erf}(\tau_k r), \end{aligned} \quad (7)$$

where  $\alpha_k = (0.25, 0.15, 0.2)$  and  $\gamma_k = (1/2, \sqrt{10}/2, \sqrt{1000}/2)$  with  $k = 1, 2, 3$  [63], and the  $\tau_k$  could be obtained by

$$\tau_k = \frac{1}{\sqrt{\frac{1}{\sigma_{ij}^2} + \frac{1}{\gamma_k^2}}}. \quad (8)$$

Additionally, the semirelativistic correction with momentum-dependent factors is introduced. For the Coulomb term, the correction is

$$G_{12}(r) \rightarrow \left( 1 + \frac{p^2}{E\bar{E}} \right)^{1/2} G_{12}(r) \left( 1 + \frac{p^2}{E\bar{E}} \right)^{1/2}. \quad (9)$$

For the spin-dependent terms, the semi-relativistic correction could be written as

$$V_{\alpha\beta}^i \rightarrow \left( \frac{m_\alpha m_\beta}{E_\alpha E_\beta} \right)^{1/2+\epsilon_i} V_{\alpha\beta} \left( \frac{m_\alpha m_\beta}{E_\alpha E_\beta} \right)^{1/2+\epsilon_i}. \quad (10)$$

The remaining terms in Eq. (6) are spin-dependent potentials, which are defined as

$$\widetilde{V}^{\text{cont}}(r) = \frac{2\mathbf{S}_1 \cdot \mathbf{S}_2}{3m_1 m_2} \nabla^2 \widetilde{G}_{12}^c(r), \quad (11)$$

$$\widetilde{V}^{\text{tens}}(r) = - \left( \frac{3\mathbf{S}_1 \cdot \mathbf{r} \mathbf{S}_2 \cdot \mathbf{r} / r^2 - \mathbf{S}_1 \cdot \mathbf{S}_2}{3m_1 m_2} \right) \left( \frac{\partial^2}{\partial r^2} - \frac{1}{r} \frac{1}{\partial r} \right) \widetilde{G}_{12}^t(r), \quad (12)$$

$$\begin{aligned} \widetilde{V}^{\text{sov}}(r) = & \frac{\mathbf{S}_1 \cdot \mathbf{L}}{2m_1^2} \frac{1}{r} \frac{\partial \widetilde{G}_{11}^{\text{sov}}(r)}{\partial r} + \frac{\mathbf{S}_2 \cdot \mathbf{L}}{2m_2^2} \frac{1}{r} \frac{\partial \widetilde{G}_{22}^{\text{sov}}(r)}{\partial r} \\ & + \frac{(\mathbf{S}_1 + \mathbf{S}_2) \cdot \mathbf{L}}{m_1 m_2} \frac{1}{r} \frac{\partial \widetilde{G}_{12}^{\text{sov}}(r)}{\partial r}. \end{aligned} \quad (13)$$

In Eqs. (11)-(13), the semirelativistic correction factors in Eq. (10) with  $\epsilon_i = \epsilon_c, \epsilon_t,$  and  $\epsilon_{\text{sov}}$  impacts the potentials  $\widetilde{V}^{\text{cont}}(r), \widetilde{V}^{\text{tens}}(r),$  and  $\widetilde{V}^{\text{sov}}(r),$  respectively<sup>1</sup>.

The second part of Eq. (2) contains a screened confinement potential and a scalar spin-orbit interaction, i.e.,

$$\widetilde{H}^{\text{conf}} = \widetilde{S}_{12} + \widetilde{V}^{\text{sos}}. \quad (14)$$

In the MGI model, the screen effect [38] is introduced, where we should make a replacement

$$br \rightarrow \frac{b(1 - e^{-\mu r})}{\mu}. \quad (15)$$

Then the  $\widetilde{S}_{12}$  in Eq. (14) is defined as

$$\widetilde{S}_{ij}(r) = \int d^3 \mathbf{r}' \rho_{ij}(\mathbf{r} - \mathbf{r}') \frac{b(1 - e^{-\mu r})}{\mu} + c, \quad (16)$$

where  $b$  is the strength of the confinement, and the  $\mu$  is a parameter to scale the screening effect. Then the scalar spin-orbit interaction could be obtained by

$$\widetilde{V}^{\text{sos}}(r) = - \frac{\mathbf{S}_1 \cdot \mathbf{L}}{2m_1^2} \frac{1}{r} \frac{\partial \widetilde{S}_{11}^{\text{sos}}(r)}{\partial r} - \frac{\mathbf{S}_2 \cdot \mathbf{L}}{2m_2^2} \frac{1}{r} \frac{\partial \widetilde{S}_{22}^{\text{sos}}(r)}{\partial r}, \quad (17)$$

where the  $\widetilde{S}_{11}^{\text{sos}}(r)$  and  $\widetilde{S}_{22}^{\text{sos}}(r)$  contain semirelativistic correction factors in Eq. (10) with  $\epsilon_i = \epsilon_{\text{sos}}$ .

In the above formula,  $\mathbf{S}_1$  and  $\mathbf{S}_2$  denote the spin of quark and antiquark, respectively.  $\mathbf{L}$  indicates the orbital momentum

TABLE I: The value of these parameters involved in the MGI model.

Parameter	Value	Parameter	Value
$m_u$ (GeV)	0.22	$m_d$ (GeV)	0.22
$m_s$ (GeV)	0.424	$b$ (GeV <sup>2</sup> )	0.229
$\epsilon_c$	-0.164	$\epsilon_{\text{sos}}$	0.9728
$\sigma_0$ (GeV)	1.8	$s$ (GeV)	3.88
$\mu$ (GeV)	0.081	$c$ (GeV)	-0.30
$\epsilon_{\text{sov}}$	0.262	$\epsilon_t$	1.993

between two quarks. More details of the MGI model can be found in Ref. [38].

The values of all parameters used in the MGI model are collected in Table. I. With these preparations, we further present the mass spectrum of light unflavored vector mesons in Fig. 2. In Refs. [23, 44, 75], the Lanzhou group performed the study of mass spectrum and two-body OZI allowed decay of the mesons in the  $\rho, \omega,$  and  $\phi$  family and discussed how to categorize these observed light vector  $\rho, \omega,$  and  $\phi$  states below 2.4 GeV collected in Particle Data Group (PDG) [76] into the  $\rho, \omega,$  and  $\phi$  family. Here, the MGI model was adopted, which was applied to study various light flavor systems, including kaon family [49],  $\phi$  states below 2.6 GeV [77], and high spin light flavor mesons [50]. When further exploring the property of these higher states of the  $\rho, \omega,$  and  $\phi$  family, we still use the MGI model for presenting the mass spectrum analysis. Here, besides reproducing the masses of these low lying states, the masses of higher states are also obtained. Our calculated result explicitly shows that there exists accumulation of these  $5S, 6S,$  and  $7S$  states of  $\rho, \omega$  and  $\phi$  mesons in the mass range from 2.4 GeV to 3 GeV.

In this work, we also calculate the dilepton decay widths of these discussed light unflavored vector mesons. The dilepton decay width of a unflavored meson can be expressed as [63]

$$\Gamma_{e^+e^-} = \frac{4\pi}{3} \alpha^2 m |\mathcal{M}|^2, \quad (18)$$

where the  $m$  is the mass of the vector meson. The  $\mathcal{M}$  in Eq. (18) is the decay amplitude. For  $S$ -wave vector mesons, we employ  $\mathcal{M}_\rho = \sqrt{6}V_\rho, \mathcal{M}_\omega = \sqrt{2/3}V_\omega,$  and  $\mathcal{M}_\phi = -\sqrt{4/3}V_\phi$  to express the decay amplitudes of the  $\rho, \omega,$  and  $\phi$  states, respectively. In potential models, the factors  $V_\rho, V_\omega,$  and  $V_\phi$  can be written as

$$V_{\rho/\omega/\phi} = m^{-2} \widetilde{m}^{1/2} (2\pi)^{-3/2} \int d^3 \mathbf{p} (4\pi)^{-1/2} \Phi(p) \left( \frac{m_1 m_2}{E_1 E_2} \right)^{1/2}, \quad (19)$$

where  $m_1$  and  $m_2$  are consistent quark masses in the meson, and  $E_1$  and  $E_2$  are energies of the quarks. The  $\Phi(p)$  in Eq. (19) is the radial part of the spatial wave function in the momentum space, which is extracted from the potential model. And the  $\widetilde{m}$  is calculated by  $\widetilde{m} = 2 \int d^3 \mathbf{p} E |\phi(\mathbf{p})|^2,$  where  $\phi(\mathbf{p}) = \Phi(p) Y_{lm}(\Omega_{\mathbf{p}})$ . Besides, we use  $M'_\rho = \sqrt{4/3}V'_\rho, M'_\omega = \sqrt{4/27}V'_\omega,$  and  $M'_\phi = -\sqrt{8/27}V'_\phi$  to denote the decay amplitudes of the  $D$ -wave vector  $\rho, \omega,$  and  $\phi$  mesons, respec-

<sup>1</sup> The spin-orbit and tensor interactions without smearing transformations may contain the  $1/r^3$  term. But for  $S$ -wave states, the spin-orbit and tensor operators are zero, thus the spin-orbit and tensor potentials do not lead to singularities.

tively. The  $V'_\rho$ ,  $V'_\omega$ , and  $V'_\phi$  could be expressed by

$$V'_{\rho/\omega/\phi} = m^{-2} \tilde{m}^{1/2} (2\pi)^{-3/2} \int d^3\mathbf{p} (4\pi)^{-1/2} \phi(\mathbf{p}) \times \left( \frac{m_1 m_2}{E_1 E_2} \right)^{1/2} \left( \frac{P}{E_1} \right)^2. \quad (20)$$

With preparations above, the dilepton decay widths of these discussed light unflavored vector mesons are calculated and presented in Table II.

TABLE II: The dilepton decay widths of the discussed light unflavored vector mesons in units of keV.

States	$\rho(5S)$	$\rho(6S)$	$\rho(7S)$	$\rho(4D)$	$\rho(5D)$	$\rho(6D)$
$\Gamma_{e^+e^-}$	0.0377	0.0204	0.0195	0.0070	0.0052	0.0029
States	$\omega(5S)$	$\omega(6S)$	$\omega(7S)$	$\omega(4D)$	$\omega(5D)$	$\omega(6D)$
$\Gamma_{e^+e^-}$	0.0042	0.0023	0.0022	0.0008	0.0006	0.0003
States	$\phi(4S)$	$\phi(5S)$	$\phi(6S)$	$\phi(3D)$	$\phi(4D)$	$\phi(5D)$
$\Gamma_{e^+e^-}$	0.0492	0.0291	0.0162	0.0096	0.0058	0.0037

In the following section, we pay more attention to their two-body OZI allowed strong decays, which can give important hints to the experimental search for them. Here, we need to emphasize that the numerical forms of the spatial wave function of these discussed light vector unflavored mesons can be obtained, which are as the input of the following discussion, by their decay behavior.

## B. Two-body OZI allowed strong decay

For calculating the two-body OZI allowed strong decay of these discussed higher unflavored vector meson states, we apply the QPC model, which is an effective approach to quantitatively estimate such physical quantity [39–41].

In the QPC model, when a meson decay occurs, a quark-antiquark pair is created from the vacuum with the quantum number  $J^{PC} = 0^{++}$  and combines with the corresponding antiquark and quark in the initial meson to produce two final mesons. In Ref. [79], the authors introduced the wave functions of the mock states when calculating the transition amplitudes. In the QPC model, the wave function of a mock state is also adopted. In the decay process  $A \rightarrow BC$ , the wave function of the mock state  $A$  is defined as [41, 79]

$$\begin{aligned} & \left| A \left( n_A^{2S_A+1} L_{AJ_A M_{J_A}} \right) (\mathbf{P}_A) \right\rangle \\ & \equiv \sqrt{2E_A} \sum_{M_{L_A}, M_{S_A}} \langle L_A M_{L_A} S_A M_{S_A} | J_A M_{J_A} \rangle \\ & \times \int d^3\mathbf{p}_A \psi_{n_A L_A M_{L_A}}(\mathbf{p}_A) \chi_{S_A M_{S_A}}^{12} \phi_A^{12} \omega_A^{12} \\ & \times \left| q_1 \left( \frac{m_1}{m_1 + m_2} \mathbf{P}_A + \mathbf{p}_A \right) \bar{q}_2 \left( \frac{m_2}{m_1 + m_2} \mathbf{P}_A - \mathbf{p}_A \right) \right\rangle, \end{aligned} \quad (21)$$

where the  $m_1$  and  $m_2$  are masses of quark  $q_1$  and antiquark  $\bar{q}_2$ , respectively. For the mock state wave function of the meson

$B(C)$ , we simply replace ‘ $A$ ’ by ‘ $B$ ’ (‘ $C$ ’) in Eq. (21). The  $n_A$  in Eq. (21) is the radial quantum number of the meson  $A$ . The  $S_A$ ,  $L_A$ , and  $J_A$  are spin, orbital angular momentum, and total angular momentum, respectively. Note that  $\mathbf{p}_A = \frac{m_1 \mathbf{p}_1 - m_2 \mathbf{p}_2}{m_1 + m_2}$  is the relative momentum of the  $q_1 \bar{q}_2$  pair, where  $\mathbf{p}_1$  and  $\mathbf{p}_2$  are the momentum of  $q_1$  and  $\bar{q}_2$ , respectively. Since the particles here are on shell, the integral variable  $\mathbf{p}_A$  in Eq. (21) is three dimensional. Note that  $\mathbf{P}_A = \mathbf{p}_1 + \mathbf{p}_2$  and  $E_A$  are total momentum and total energy of the meson  $A$ , respectively. The  $\psi_{n_A L_A M_{L_A}}(\mathbf{p}_A)$  is the spatial wave function in momentum space. The  $\chi_{S_A M_{S_A}}^{12}$ ,  $\phi_A^{12}$ , and  $\omega_A^{12}$  are the spin, flavor, and color wave functions, respectively.

The total decay width in the center-of-mass (CM) frame is given by

$$\Gamma = \frac{\pi}{4} \frac{|\mathbf{P}|}{M_A^2} \sum_{LS} |M^{LS}|^2. \quad (22)$$

Here,  $\mathbf{P}$  is the momentum outgoing meson (meson  $B$  or meson  $C$ ).  $M_A$  is the mass of meson  $A$ .  $\mathbf{L}$  and  $\mathbf{S}$  denote the relative orbital angular and total spin momentum between meson  $B$  and  $C$ , respectively.  $M^{LS}$  denotes the partial wave amplitude and is related to the helicity amplitude  $M^{M_{J_A} M_{J_B} M_{J_C}}$  according to Jacob-Wick formula [80]. In the CM frame, the specific form of  $M^{M_{J_A} M_{J_B} M_{J_C}}$  can be written as

$$\begin{aligned} & M^{M_{J_A} M_{J_B} M_{J_C}}(\mathbf{P}) \\ & = \gamma \sqrt{8E_A E_B E_C} \sum_{M_{L_A}, M_{S_A}, M_{L_B},} \\ & \quad M_{S_B}, M_{L_C}, M_{S_C}, m \\ & \times \langle L_B M_{L_B} S_B M_{S_B} | J_B M_{J_B} \rangle \langle L_C M_{L_C} S_C M_{S_C} | J_C M_{J_C} \rangle \\ & \times \langle 1m1 - m | 00 \rangle \langle \chi_{S_B M_{S_B}}^{14} \chi_{S_C M_{S_C}}^{32} | \chi_{S_A M_{S_A}}^{12} \chi_{1-m}^{34} \rangle \\ & \times \left[ \langle \phi_B^{14} \phi_C^{32} | \phi_A^{12} \phi_0^{34} \rangle I(\mathbf{P}, m_2, m_1, m_3) \right. \\ & \left. + (-1)^{1+S_A+S_B+S_C} \langle \phi_B^{32} \phi_C^{14} | \phi_A^{12} \phi_0^{34} \rangle I(-\mathbf{P}, m_2, m_1, m_3) \right], \end{aligned} \quad (23)$$

where  $\gamma$  as the strength of the quark-antiquark pair created from the vacuum is fixed to be 6.57 [77].  $\phi_0$  denotes the flavor wave function of this quark-antiquark pair. Note that  $I(\mathbf{P}, m_2, m_1, m_3)$  is the momentum space integral

$$\begin{aligned} I(\mathbf{P}, m_2, m_1, m_3) & = \int d^3\mathbf{p} \psi_{n_B L_B M_{L_B}}^* \left( \frac{m_3}{m_1 + m_3} \mathbf{P} + \mathbf{p} \right) \\ & \times \psi_{n_C L_C M_{L_C}}^* \left( \frac{m_3}{m_2 + m_3} \mathbf{P} + \mathbf{p} \right) \\ & \times \psi_{n_A L_A M_{L_A}}(\mathbf{P} + \mathbf{p}) \mathcal{Y}_1^m(\mathbf{p}), \end{aligned} \quad (24)$$

where  $\mathcal{Y}_1^m(\mathbf{p})$  is a solid harmonic that gives the momentum space distribution of the created quark-antiquark pair.

In our previous works, the QPC model was employed to deal with the two-body OZI allowed strong decays of light unflavored vector mesons, which include  $\omega(2S)$ ,  $\omega(1D)$ ,  $\phi(2S)$ , and  $\phi(2D)$  [23] and  $\rho(2S)$ ,  $\rho(3S)$ ,  $\rho(4S)$ ,  $\rho(1D)$ ,  $\rho(2D)$ , and  $\rho(3D)$  [44], where the experimental widths have been well reproduced. In addition, we predicted the partial and total

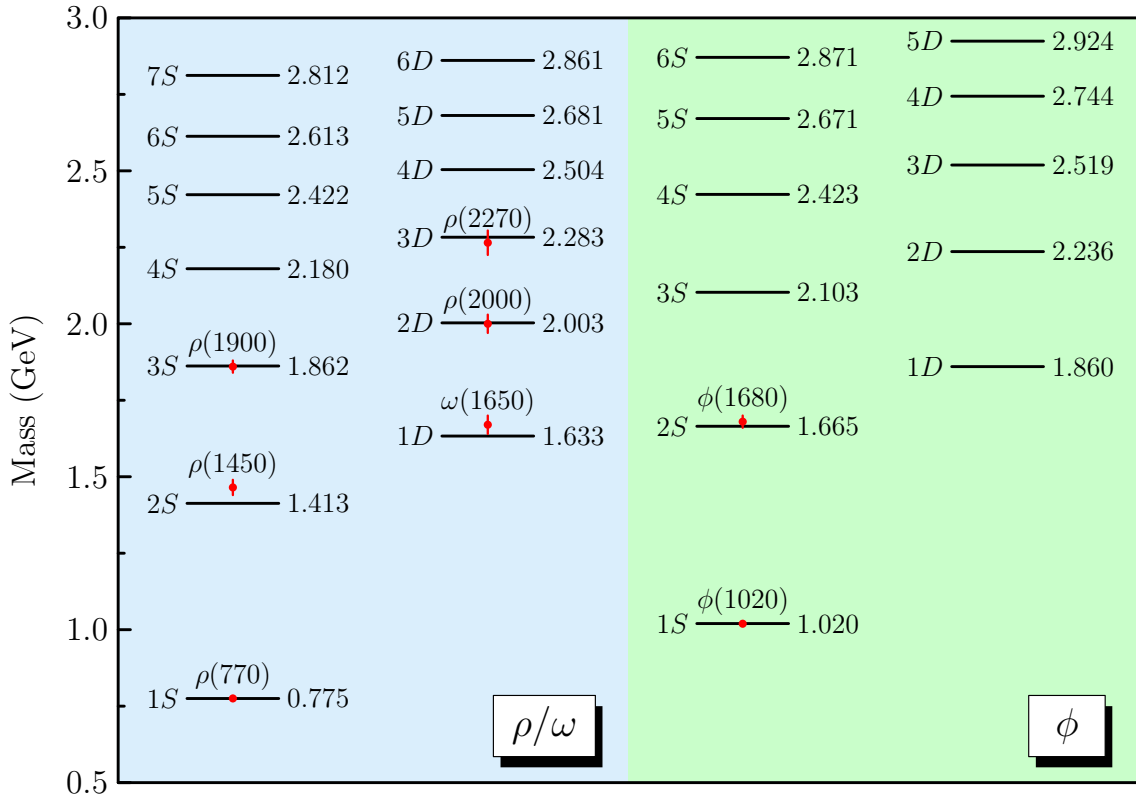


FIG. 2: The comparison of calculated results calculated in this work and the experimental data of mass of higher  $\rho$ ,  $\omega$  and  $\phi$  states. Here, the red dots denote the experimental data from Refs. [28, 34, 76, 78].

widths of the  $\phi(1D)$ ,  $\omega(2D)$ ,  $\phi(3S)$ , and  $\omega(3S)$  states [23]. Until now, these excited light unflavored vector mesons below 2.4 GeV have been systemically studied. Thus, in the present work, we do not list the results of these low-lying states.

Focusing on the light unflavored vector mesons existing in the range of 2.4 ~ 3 GeV, we continue to adopt the QPC model to estimate the strong decay widths, which is a main task of the following subsections.

### 1. $\rho$ states

As shown in Fig. 2, there are six  $\rho$  states [ $\rho(5S)$ ,  $\rho(6S)$ ,  $\rho(7S)$ ,  $\rho(4D)$ ,  $\rho(5D)$ , and  $\rho(6D)$ ] existing in the mass range of 2.4 ~ 3 GeV.

The obtained total and main partial decay widths of  $\rho(5S)$  are shown in Fig. 3, which show that  $\pi a_2(1700)$  is the dominant decay channel and the total width of  $\rho(5S)$  can reach up to 81.85 MeV. In Fig. 3, we also list their several typical decay modes like  $\pi\pi$  and  $\pi\omega$  easily accessible at experiment. However, the branching ratios of these typical decays are not obvious. Of course, the  $\rho(5S)$  state can also decay into an open-strange meson pair. However, our result shows that their contribution to the total width is not significant. For example,  $\rho(5S) \rightarrow KK_1(1270)$  and  $K^*K_1(1270)$ , have branching ratios of 0.43% and 0.41%, respectively. Thus, in this work, we do not collect the decay channels relevant to the open-strange

meson pair in Fig. 3.

The predicted decay behavior of  $\rho(6S)$  is given in Fig. 4. Similar to the  $\rho(5S)$  state, its dominant decay channel is also  $\pi a_2(1700)$ , while the  $\rho\rho(1450)$ ,  $\pi\pi_2(1880)$ ,  $\pi\pi(1800)$  and  $\pi\pi(1300)$  modes have sizable contributions to the total decay width, which is predicted to be around 57.25 MeV. Additionally, the particle widths of  $KK_1(1270)$  and  $K^*K_1(1270)$  are 0.18 MeV and 0.16 MeV, respectively, which are not listed in Fig. 3.

The calculation results for the  $\rho(7S)$  are presented in Fig. 3, where  $\rho\rho(1450)$  and  $\pi\pi_2(1880)$  are its dominant decay modes. In addition, the contribution of the  $\pi\pi(1800)$ ,  $\pi a_2(1700)$ ,  $\pi\pi(1300)$  and  $\rho\rho$  decay modes to total width cannot be ignored. As the typical channels,  $\pi\pi$  and  $\pi\omega$  have the branching ratios of 1.09% and 0.10%, respectively.

Accompanying with these three  $S$ -wave states, three corresponding  $D$ -wave states exist in the same mass range. In Fig. 3, the two-body OZI allowed strong decay behavior of  $\rho(4D)$ ,  $\rho(5D)$ , and  $\rho(6D)$  are given by presenting the total decay width and the branching ratios of their partial decays. The total decay widths of  $\rho(4D)$ ,  $\rho(5D)$ , and  $\rho(6D)$  are 92.33 MeV, 55.69 MeV, and 32.96 MeV, respectively, where their main decay modes are  $\pi\pi_2(1880)$ ,  $\pi\pi(1300)$  and  $\pi\pi(1800)$ . Since these three  $D$ -wave  $\rho$  states have sizable  $\pi\pi$  decay rates, the  $e^+e^- \rightarrow \pi\pi$  process can be as the ideal channel to identify these  $D$ -wave  $\rho$  states, which should stimulate experimentalists' interest in measuring the cross section of  $e^+e^- \rightarrow \pi\pi$  with

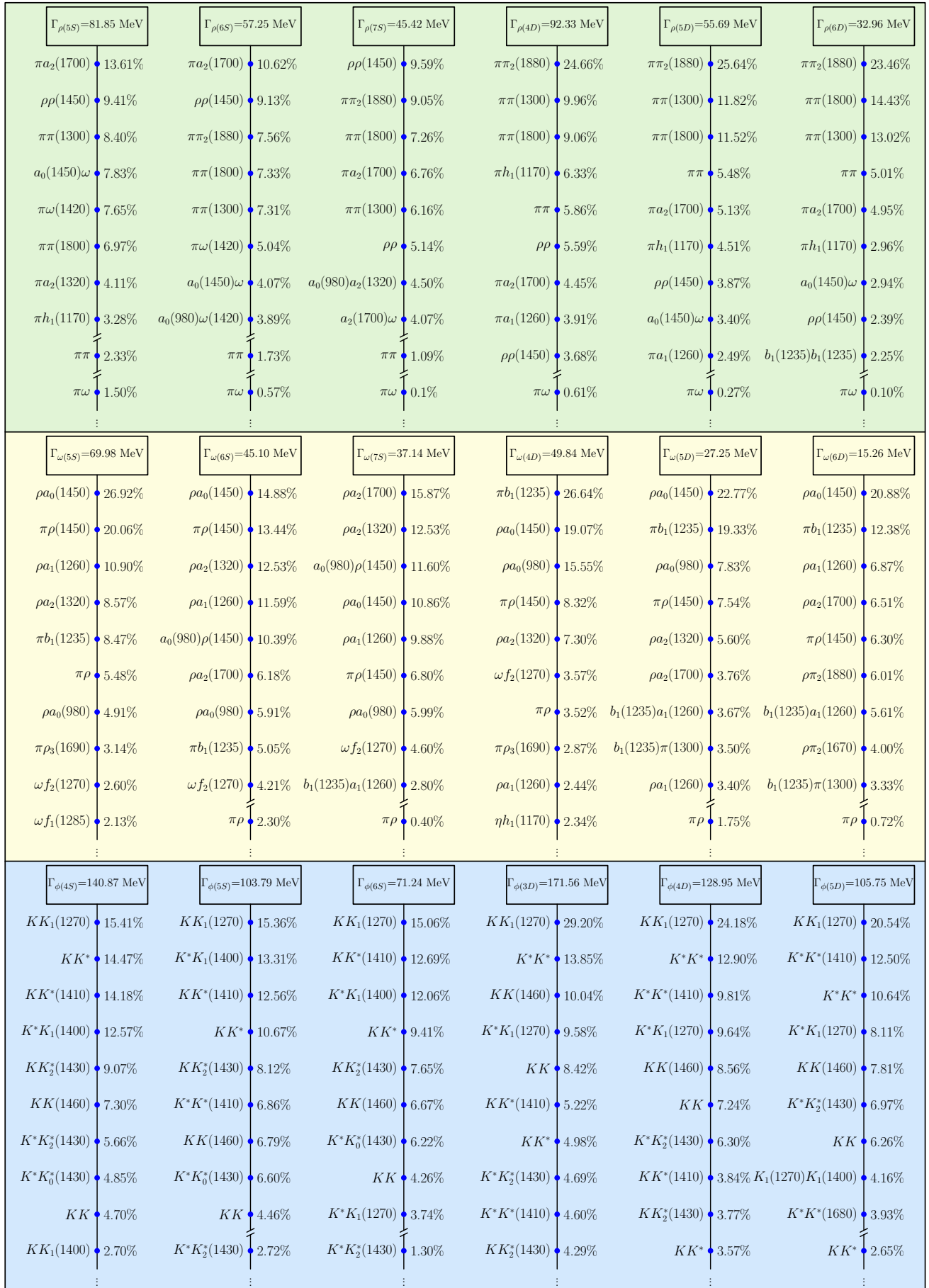


FIG. 3: The two-body strong decay behaviors of these discussed light vector mesons with the mass range from 2.4 GeV to 3 GeV. Here, we show their branching ratio of main channels and the total decay width.

energy of collision up to 3 GeV.

## 2. $\omega$ states

In the following, we check the two-body OZI allowed strong decay of six higher  $\omega$  mesonic states, which include  $\omega(5S)$ ,  $\omega(6S)$ ,  $\omega(7S)$ ,  $\omega(4D)$ ,  $\omega(5D)$ , and  $\omega(6D)$ , where their total decay widths and partial decay widths estimated by the QPC model are shown in Fig. 3.

The total widths of  $\omega(5S)$  and  $\omega(6S)$ , which are contributed by the main decay channels like  $\rho a_0(1450)$ ,  $\pi\rho(1450)$ ,  $\rho a_1(1260)$ , and  $\rho a_2(1320)$ , are 69.98 MeV and 45.10 MeV, respectively. It is worth noting that the typical mode  $\pi\rho$  has sizable contribution to the total width. Thus,  $e^+e^-$  annihilation into  $\pi\rho$  is a perfect process to experimentally search for these  $\omega$  states. Similar to the situation of the discussed  $\rho$  states,  $\omega(5S)$  and  $\omega(6S)$  decaying into an open-strange meson pair are not significant.

The decay properties of  $\omega(7S)$  we predicted are presented in Fig. 3, where its dominant decay mode is the  $\rho a_2(1700)$  channel. Other main decay modes of  $\omega(7S)$  include  $\rho a_2(1320)$ ,  $a_0(980)\rho(1450)$ ,  $\rho a_0(1450)$ , and  $\rho a_1(1260)$ . These partial decay widths of  $\omega(7S)$  into an open-strange meson pair are tiny in our calculation, which are not shown here.

Additionally, we also study three  $D$ -wave  $\omega$  states existing in the mass range 2.4 ~ 3 GeV. The estimated total decay width and branching ratios of partial decay of  $\omega(4D)$ ,  $\omega(5D)$ , and  $\omega(6D)$  are listed in Fig. 3, where the obtained total width of  $\omega(4D)$ ,  $\omega(5D)$ , and  $\omega(6D)$  are 49.84 MeV, 27.25 MeV, and 15.26 MeV, respectively. These  $D$ -wave  $\omega$  states mainly decay into  $\pi b_1(1235)$ , and  $\rho a_0(1450)$ . Other decay channels like  $\pi\rho(1450)$  and  $\rho a_0(980)$  also have a non-negligible effect on their total decay widths. Additionally,  $\omega(4D)$  and  $\omega(5D)$  all have sizable  $\pi\rho$  decay rates, which are more significant than  $\omega(6D)$ .

## 3. $\phi$ states

In this subsection, we discuss two-body strong decays of  $\phi(4S)$ ,  $\phi(5S)$ ,  $\phi(6S)$ ,  $\phi(3D)$ ,  $\phi(4D)$ , and  $\phi(5D)$ , which are also listed in Fig. 3.

From Fig. 3, we can notice that the main decay channels of  $\phi(4S)$ ,  $\phi(5S)$  and  $\phi(6S)$  are  $KK_1(1270)$ ,  $KK^*$ ,  $KK^*(1410)$ , and  $K^*K_1(1400)$ , where the total decay widths of them are 140.87 MeV, 103.79 MeV, and 71.24 MeV, respectively. Due to the sizable contribution of the channel  $KK^*$  to the total decay widths of these discussed  $\phi$  states, exploring  $S$ -wave  $\phi$  mesonic states via the  $e^+e^- \rightarrow KK^*$  process is suggested.

In the same mass range, there are three  $D$ -wave  $\phi$  mesons. In this work, we also estimate their decay behaviors.  $\phi(3D)$  has the total width of 171.56 MeV, where the branching ratio of its  $KK_1(1270)$  decay channel is 29.20%, which is the main decay channel. Other modes including  $K^*K^*$ ,  $KK(1460)$ ,  $K^*K_1(1270)$ , and  $KK$  are also significant. The predicted total width of  $\phi(4D)$  is 128.95 MeV. The channels of  $KK_1(1270)$ ,

$K^*K^*$ ,  $K^*K^*(1410)$ , and  $K^*K_1(1270)$  have the branching ratios of 24.18%, 12.90%, 9.81%, and 9.64%, respectively. And then, the obtained total decay width of  $\phi(5D)$  is 95.12 MeV in this work. The results presented in Fig. 3 further indicate that the branching ratio of the  $\phi(5D)$  decays into  $KK_1(1270)$ ,  $K^*K^*(1410)$ ,  $K^*K^*$ , and  $K^*K_1(1270)$  can reach up to 20.54%, 12.50%, 10.64%, and 8.11%, respectively.

Through the theoretical calculation given in this work, we find that the decay mode  $K^*K_2^*(1430)$  of the six  $\phi$  states discussed above has a significant contribution to their total decay widths. Thus, measuring the cross section of  $e^+e^- \rightarrow K_2^*(1430)K\pi$  with energy of collision up to 3 GeV will be a promising approach to identify these highly excited  $\phi$  states. As shown in Fig. 4 (c), indeed there are many obvious enhancement structures existing in the collision energy range of 2.4~2.7 GeV for  $e^+e^- \rightarrow K_2^{*0}(1430)K^-\pi^+$ , which may correspond to these discussed  $\phi$  mesons. More precise data is expected in future experiments.

## III. EXPERIMENTAL EVIDENCE

When having the theoretical results of masses of these higher states of light unflavored vector mesons, we can make comparison of our results with the experimental data as shown in Fig. 4. Firstly, focusing on the data of  $e^+e^- \rightarrow \omega\pi^+\pi^-\pi^0$  [34], which has a close relation with higher  $\rho$  mesons due to the  $G$ -parity conservation, we find that the invariant mass distribution shows obvious enhancement structures like the event accumulation around 2.65 GeV. This broad structure overlaps with the predicted  $\rho(6S)$  and  $\rho(5D)$  states. There exists a jump point around 2.76 GeV, which may corresponds to  $\rho(7S)$ . And then, an unnotable fluctuation around 2.81 GeV just locates at the position of  $\rho(6D)$ . Additionally, a bump structure around 2.4 GeV should have relation with  $\rho(5S)$ , while around the  $\rho(4D)$  state we can also find an obvious jump point.

The data of  $e^+e^- \rightarrow \pi^+\pi^-\pi^0$  [35] is an ideal process to identify  $\omega$  states. Although we mark these predicted  $\omega$  states in the corresponding cross section data, we cannot identify the obvious bump structure corresponding to these states since the precision of the measured data is not enough. Thus, we have to wait for further precise measurements of the cross section of  $e^+e^- \rightarrow \pi^+\pi^-\pi^0$ .

In the following, we check four measured processes  $e^+e^- \rightarrow K_2^{*0}(1430)K^-\pi^+$  [36],  $e^+e^- \rightarrow \phi\pi^+\pi^-$  [37],  $e^+e^- \rightarrow \phi f_0(980)$  [37], and  $e^+e^- \rightarrow \phi f_2(1525)$  [36]. For  $e^+e^- \rightarrow K_2^{*0}(1430)K^-\pi^+$ , there exists abundant event clusters. Since these predicted higher  $\rho$ ,  $\omega$  and  $\phi$  states can decay into open-strange meson pairs, it is difficult to distinguish  $\rho$ ,  $\omega$  and  $\phi$  states via the  $e^+e^- \rightarrow K_2^{*0}(1430)K^-\pi^+$  channel. Further data analysis of  $e^+e^- \rightarrow K_2^{*0}(1430)K^-\pi^+$  is an interesting research issue similar to the way adopted in Refs. [18, 75].

Different from  $e^+e^- \rightarrow K_2^{*0}(1430)K^-\pi^+$ ,  $e^+e^- \rightarrow \phi f_0(980)$  can be the ideal process to identify these higher  $\phi$  states. Two obvious structures around 2.4 GeV and 2.7 GeV may correspond to  $\phi(4S)$  and  $\phi(5S)$ , respectively. Of course, we may also find an event accumulation around 2.5 GeV corresponding to  $\phi(3D)$ . For  $e^+e^- \rightarrow \phi\pi^+\pi^-$ , the structure at 2.41 GeV

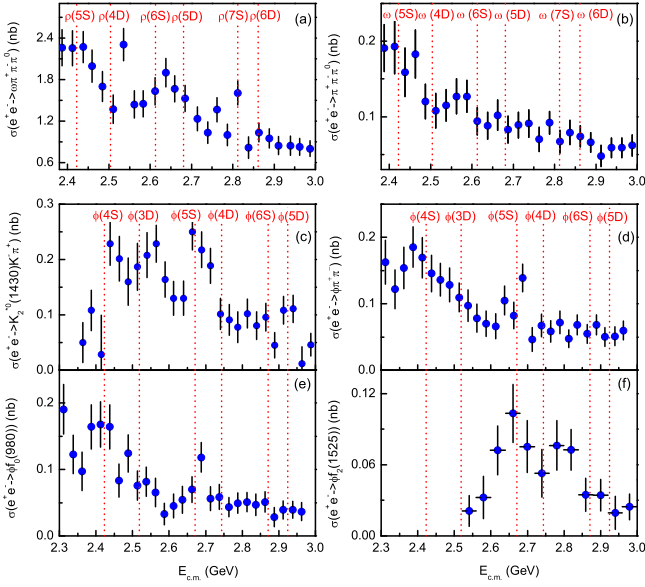


FIG. 4: A comparison of theoretical masses of these discussed light vector meson  $\rho$ ,  $\omega$  and  $\phi$  mesons and the experimental data of  $e^+e^- \rightarrow \omega\pi^+\pi^-\pi^0$  [34],  $e^+e^- \rightarrow \pi^+\pi^-\pi^0$  [35],  $e^+e^- \rightarrow K_2^{*0}(1430)K^-\pi^+$  [36],  $e^+e^- \rightarrow \phi\pi^+\pi^-$  [36],  $e^+e^- \rightarrow \phi f_0(980)$  [36], and  $e^+e^- \rightarrow \phi f_2(1525)$  [36]. These observed light vector  $\rho$ ,  $\omega$ , and  $\phi$  states below 2.4 GeV collected in PDG [76] have been studied in our previous work [23, 44, 75]. Thus, here we do not list these light vector  $\rho$ ,  $\omega$ , and  $\phi$  states below 2.4 GeV.

and the enhancement around 2.7 GeV may have relation to the  $\phi(4S)$ ,  $\phi(5S)/\phi(4D)$ . For  $e^+e^- \rightarrow \phi\pi^+\pi^-$ , the broad structure around 2.65 GeV contains the information of the predicted  $\phi(5S)/\phi(4D)$ .

In fact, this simple comparison of the experimental data and masses of these discussed vector states only reflects some possible evidences of these predicted higher states of light unflavored vector meson. For further illustrating it, in the following, we take two processes  $e^+e^- \rightarrow \omega\pi^+\pi^-\pi^0$  and  $e^+e^- \rightarrow \phi f_0(980)$  as examples to make further analysis.

In general, the cross section can be parametrized as the coherent sum of an  $s$ -dependent continuum amplitude and a resonant amplitude described by a Breit-Wigner function [81], i.e.,

$$\sigma(s) = \left| a e^{-b(\sqrt{s}-M_{th})} + \sum_R BW_R(\sqrt{s}) e^{i\phi_R} \right|^2, \quad (25)$$

where  $a$  and  $b$  are the continuum parameters,  $M_{th}$  is the sum of the masses of the final state particles, and  $\phi_R$  is the phase angle between the amplitudes. The Breit-Wigner function is given by

$$BW_R(\sqrt{s}) = \frac{\sqrt{12\pi\Gamma_R^{e^+e^-}\mathcal{B}_R\Gamma_R^{\text{tot}}}}{s - M_R^2 + iM_R\Gamma_R^{\text{tot}}}, \quad (26)$$

where  $M_R$ ,  $\Gamma_R^{e^+e^-}$ , and  $\Gamma_R^{\text{tot}}$  denote the mass, partial width to

$e^+e^-$ , and total width of the assumed intermediate resonance  $R$ .  $\mathcal{B}_R$  is the branching ratio for  $R \rightarrow$  (final states).

TABLE III: The fitting parameters of depicting the Born cross section of  $e^+e^- \rightarrow \omega\pi^+\pi^-\pi^0$ .

Parameters	Solution
$\Gamma_{e^+e^-}\mathcal{B}(\rho(5S) \rightarrow \omega\pi^+\pi^-\pi^0)$ (eV)	$3.38 \pm 0.96$
$\Gamma_{e^+e^-}\mathcal{B}(\rho(6S) \rightarrow \omega\pi^+\pi^-\pi^0)$ (eV)	$0.62 \pm 0.44$
$\Gamma_{e^+e^-}\mathcal{B}(\rho(5D) \rightarrow \omega\pi^+\pi^-\pi^0)$ (eV)	$0.86 \pm 0.52$
$\Gamma_{e^+e^-}\mathcal{B}(\rho(6D) \rightarrow \omega\pi^+\pi^-\pi^0)$ (eV)	$0.96 \pm 0.52$
$\phi_{\rho(5S)}$ (rad)	$4.76 \pm 0.21$
$\phi_{\rho(6S)}$ (rad)	$3.92 \pm 0.44$
$\phi_{\rho(5D)}$ (rad)	$5.52 \pm 0.35$
$\phi_{\rho(6D)}$ (rad)	$5.20 \pm 0.38$
$a$ ( $\times 10^{-3}$ GeV $^{-2}$ )	$-4.08 \pm 0.05$
$b$	$0.54 \pm 0.01$
$\chi^2/\text{d.o.f}$	0.60

TABLE IV: The fitting parameters of depicting the Born cross section of  $e^+e^- \rightarrow \phi f_0(980)$ .

Parameters	Solution
$\Gamma_{e^+e^-}\mathcal{B}(\phi(5S) \rightarrow \phi f_0(980))$ (eV)	$1.36 \pm 0.31$
$\Gamma_{e^+e^-}\mathcal{B}(\phi(6S) \rightarrow \phi f_0(980))$ (eV)	$0.94 \pm 0.32$
$\phi_{\phi(5S)}$ (rad)	$4.32 \pm 0.21$
$\phi_{\phi(6S)}$ (rad)	$3.86 \pm 0.17$
$a$ ( $\times 10^{-3}$ GeV $^{-2}$ )	$-0.92 \pm 0.004$
$b$	$1.92 \pm 0.09$
$\chi^2/\text{d.o.f}$	0.49

With this preparation, we first fit the measured cross section of  $e^+e^- \rightarrow \omega\pi^+\pi^-\pi^0$  [34]. The comparison in Fig. 4 (a) indicates that  $\rho(5S)$ ,  $\rho(6S)$ ,  $\rho(5D)$  and  $\rho(6D)$  should be considered in our fit, where the resonance parameters for these vector states are taken from our calculation given in Sec. II and the fitted parameters are listed in Table III. As shown in Fig. 5 (a), we can depict the data of the cross section of  $e^+e^- \rightarrow \omega\pi^+\pi^-\pi^0$  [34], by which the values of  $\Gamma_R^{e^+e^-}\mathcal{B}_R$  for these considered light unflavored vector mesons can be obtained. This information is valuable to further study around these light unflavored vector mesons.

Along this line, we may study the  $e^+e^- \rightarrow \phi f_0(980)$  process [36]. The fitted result can be found in Fig. 5 (b). When considering the contributions from  $\phi(5S)$  and  $\phi(6S)$ , we can describe the experimental data well, where the fitting parameters are listed in Table IV.

We expect more precise data, which can be applied to identify these discussed higher light unflavored vector mesons.

#### IV. SUMMARY

In the past decades, the process of  $e^+e^-$  annihilation into light mesons can be as an ideal platform to probe the light vector mesonic state. A typical example is the observation of  $Y(2175)$ , which had stimulated theorists' interest in revealing its inner structure [17–22]. In recent years, BESIII, as the

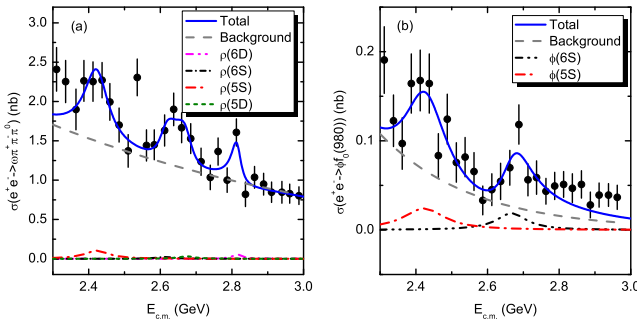


FIG. 5: The fitted result of the cross section of (a)  $e^+e^- \rightarrow \omega\pi^+\pi^-\pi^0$  and (b)  $e^+e^- \rightarrow \phi f_0(980)$ . The black dots with the error bar are experimental data [34, 36].

main force of studying light hadron spectroscopy, has accumulated more and more data of  $e^+e^-$  annihilation into light mesons [35, 81–88]. Especially, these experimental measurements from BESIII make that constructing light unflavored vector mesons around 2 GeV become possible [18, 75, 86–88].

Although big progress has been made by both experimentalists and theorists, our knowledge of these light unflavored vector mesons existing in the mass range of 2.4 ~ 3 GeV is not abundant, which inspires our attention.

In this work, we obtain the masses and decay widths of these discussed higher  $\rho$ ,  $\omega$ , and  $\phi$  states in the 2.4 ~ 3 GeV mass range and make a rough comparison with the present ex-

perimental data as shown in Fig. 4. Although the present precision of experimental data is not enough to conclude whether these event clusters can be identified as these predicted states, we still want to show this possible evidence. With the improvement of experimental precision, we suggest our experimental colleagues pay attention to these predicted higher vector states.

As emphasized in the recent white paper released by BESIII [51], the study around light hadrons will still be one of the tasks of the BESIII experiment in the next ten years. According to our study, we strongly suggest our experimental colleagues pay attention to the 2.4 ~ 3 GeV energy range of collision, which has a close relation to these predicted light unflavored vector meson states.

### Acknowledgments

L.-M.W. would like to thank Lanzhou Center for Theoretical Physics to support his stay at Lanzhou University, where this work was finished. Additionally, L.-M. W. would like to thank Qin-Song Zhou for his help of fitting the experimental data. This work is supported by the China National Funds for Distinguished Young Scientists under Grant No. 11825503, National Key Research and Development Program of China under Contract No. 2020YFA0406400, the 111 Project under Grant No. B20063, the National Natural Science Foundation of China under Grant No. 12047501, and the projects funded by Science and Technology Department of Qinghai Province Project No. 2020-ZJ-728.

- 
- [1] M. Gell-Mann, A Schematic Model of Baryons and Mesons, Phys. Lett. **8**, 214-215 (1964).
  - [2] G. Zweig, An SU(3) model for strong interaction symmetry and its breaking. Version 1, CERN-TH-401.
  - [3] M. J. Teper, Glueball masses and other physical properties of SU(N) gauge theories in D = (3+1): A Review of lattice results for theorists, [arXiv:hep-th/9812187 [hep-th]].
  - [4] C. A. Meyer and E. S. Swanson, Hybrid Mesons, Prog. Part. Nucl. Phys. **82**, 21-58 (2015).
  - [5] H. X. Chen, W. Chen, X. Liu and S. L. Zhu, The hidden-charm pentaquark and tetraquark states, Phys. Rept. **639**, 1-121 (2016).
  - [6] Y. R. Liu, H. X. Chen, W. Chen, X. Liu and S. L. Zhu, Pentaquark and Tetraquark states, Prog. Part. Nucl. Phys. **107**, 237-320 (2019).
  - [7] M. Ablikim *et al.* [BES Collaboration], Observation of a resonance X(1835) in  $J/\psi \rightarrow \gamma\pi^+\pi^-\eta'$ , Phys. Rev. Lett. **95**, 262001 (2005).
  - [8] M. Ablikim *et al.* [BESIII Collaboration], Confirmation of the X(1835) and observation of the resonances X(2120) and X(2370) in  $J/\psi \rightarrow \gamma\pi^+\pi^-\eta'$ , Phys. Rev. Lett. **106**, 072002 (2011).
  - [9] M. Ablikim *et al.* [BESIII Collaboration], Observation of an anomalous line shape of the  $\eta'\pi^+\pi^-$  mass spectrum near the  $p\bar{p}$  mass threshold in  $J/\psi \rightarrow \gamma\eta'\pi^+\pi^-$ , Phys. Rev. Lett. **117**, no. 4, 042002 (2016).
  - [10] M. Ablikim *et al.* [BES Collaboration], Observation of Y(2175) in  $J/\psi \rightarrow \eta\phi f_0(980)$ , Phys. Rev. Lett. **100**, 102003 (2008).
  - [11] M. Ablikim *et al.* [BESIII Collaboration], Study of  $J/\psi \rightarrow \eta\phi\pi^+\pi^-$  at BESIII, Phys. Rev. D **91**, no. 5, 052017 (2015).
  - [12] J. P. Lees *et al.* [BaBar Collaboration], Cross Sections for the Reactions  $e^+e^- \rightarrow K^+K^-\pi^+\pi^-$ ,  $K^+K^-\pi^0\pi^0$ , and  $K^+K^-K^+K^-$  Measured Using Initial-State Radiation Events, Phys. Rev. D **86**, 012008 (2012).
  - [13] B. Aubert *et al.* [BaBar Collaboration], Measurements of  $e^+e^- \rightarrow K^+K^-\eta$ ,  $K^+K^-\pi^0$  and  $K_s^0K^\pm\pi^\mp$  cross-sections using initial state radiation events, Phys. Rev. D **77**, 092002 (2008).
  - [14] C. P. Shen *et al.* [Belle Collaboration], Observation of the  $\phi(1680)$  and the Y(2175) in  $e^+e^- \rightarrow \phi\pi^+\pi^-$ , Phys. Rev. D **80**, 031101 (2009).
  - [15] B. Aubert *et al.* [BaBar Collaboration], The  $e^+e^- \rightarrow K^+K^-\pi^+\pi^-$ ,  $K^+K^-\pi^0\pi^0$  and  $K^+K^-K^+K^-$  cross-sections measured with initial-state radiation, Phys. Rev. D **76**, 012008 (2007).
  - [16] B. Aubert *et al.* [BaBar Collaboration], A Structure at 2175-MeV in  $e^+e^- \rightarrow \phi f_0(980)$  Observed via Initial-State Radiation, Phys. Rev. D **74**, 091103 (2006).
  - [17] G. J. Ding and M. L. Yan, Y(2175): Distinguish Hybrid State from Higher Quarkonium, Phys. Lett. B **657**, 49 (2007).
  - [18] J. Z. Wang, L. M. Wang, X. Liu and T. Matsuki, Deciphering the light vector meson contribution to the cross sections of  $e^+e^-$  annihilations into the open-strange channels through a combined

- analysis, Phys. Rev. D **104**, no.5, 054045 (2021).
- [19] Z. G. Wang, Analysis of the  $Y(2175)$  as a tetraquark state with QCD sum rules, Nucl. Phys. A **791**, 106 (2007).
- [20] A. Martinez Torres, K. P. Khemchandani, L. S. Geng, M. Napsuciale and E. Oset, The  $X(2175)$  as a resonant state of the  $\phi K\bar{K}$  system, Phys. Rev. D **78**, 074031 (2008).
- [21] H. X. Chen, X. Liu, A. Hosaka and S. L. Zhu, The  $Y(2175)$  State in the QCD Sum Rule, Phys. Rev. D **78**, 034012 (2008).
- [22] E. Klempt and A. Zaitsev, Glueballs, Hybrids, Multiquarks. Experimental facts versus QCD inspired concepts, Phys. Rept. **454**, 1 (2007).
- [23] X. Wang, Z. F. Sun, D. Y. Chen, X. Liu and T. Matsuki, Non-strange partner of strangeonium-like state  $Y(2175)$ , Phys. Rev. D **85**, 074024 (2012).
- [24] T. Barnes, N. Black and P. R. Page, Strong decays of strange quarkonia, Phys. Rev. D **68**, 054014 (2003).
- [25] A. Antonelli *et al.* [FENICE Collaboration], Measurement of the total  $e^+e^- \rightarrow \text{hadrons}$  cross-section near the  $e^+e^- \rightarrow N\bar{N}$  threshold, Phys. Lett. B **365**, 427 (1996).
- [26] A. B. Clegg and A. Donnachie,  $\rho$ 's in 6  $\pi$  States From Materialization of Photons, Z. Phys. C **45**, 677 (1990).
- [27] A. Hasan and D. V. Bugg, Amplitudes for  $p\bar{p} \rightarrow \pi\pi$  from 0.36-GeV/c to 2.5-GeV/c, Phys. Lett. B **334**, 215 (1994).
- [28] D. V. Bugg, Four sorts of meson, Phys. Rept. **397**, 257 (2004).
- [29] M. Atkinson *et al.* [Omega Photon Collaboration], Evidence for a  $\omega\rho^+\pi^+$  State in Diffractive Photoproduction, Z. Phys. C **29**, 333 (1985).
- [30] S. U. Chung *et al.*, Exotic and  $q\bar{q}$  resonances in the  $\pi^+\pi^-\pi^-$  system produced in  $\pi^-p$  collisions at 18-GeV/c, Phys. Rev. D **65**, 072001 (2002).
- [31] A. V. Anisovich *et al.*,  $I = 0, C = -1$  mesons from 1940 to 2410 MeV, Phys. Lett. B **542**, 19 (2002).
- [32] D. V. Bugg, Partial wave analysis of  $\bar{p}p \rightarrow \bar{\Lambda}\Lambda$ , Eur. Phys. J. C **36**, 161 (2004).
- [33] M. Atkinson *et al.* [Omega Photon Collaboration], photon diffractive dissociation to  $\rho\rho\pi$  and  $\rho\pi\pi\pi$  states, Z. Phys. C **38**, 535 (1988).
- [34] B. Aubert *et al.* [BaBar], The  $e^+e^- \rightarrow 3(\pi^+\pi^-), 2(\pi^+\pi^-\pi^0)$  and  $K^+K^-2(\pi^+\pi^-)$  cross sections at center-of-mass energies from production threshold to 4.5-GeV measured with initial-state radiation, Phys. Rev. D **73**, 052003 (2006).
- [35] M. Ablikim *et al.* [BESIII], Measurement of the  $e^+e^- \rightarrow \pi^+\pi^-\pi^0$  Cross Section from 0.7 GeV to 3.0 GeV via Initial-State Radiation, [arXiv:1912.11208 [hep-ex]].
- [36] J. P. Lees *et al.* [BaBar], Cross Sections for the Reactions  $e^+e^- \rightarrow K^+K^-\pi^+\pi^-, K^+K^-\pi^0\pi^0, K^+K^-K^+K^-$  Measured Using Initial-State Radiation Events, Phys. Rev. D **86**, 012008 (2012).
- [37] C. P. Shen *et al.* [Belle], Observation of the  $\phi(1680)$  and the  $Y(2175)$  in  $e^+e^- \rightarrow \phi\pi^+\pi^-$ , Phys. Rev. D **80**, 031101 (2009).
- [38] Q. T. Song, D. Y. Chen, X. Liu and T. Matsuki, Charmed-strange mesons revisited: mass spectra and strong decays, Phys. Rev. D **91**, 054031 (2015).
- [39] A. V. Anisovich, V. V. Anisovich, V. N. Markov, M. A. Matveev, V. A. Nikonov and A. V. Sarantsev, Radiative decays of quarkonium states, momentum operator expansion and nilpotent operators, J. Phys. G **31**, 1537 (2005).
- [40] W. Roberts and B. Silvestre-Brac, General method of calculation of any hadronic decay in the  $p$  wave triplet model, Acta Phys. Austriaca **11**, 171 (1992).
- [41] H. G. Blundell, Meson properties in the quark model: A look at some outstanding problems, [arXiv:hep-ph/9608473 [hep-ph]] (1996).
- [42] L. M. Wang, Q. S. Zhou, C. Q. Pang and X. Liu, Potential higher radial excitations in the light pseudoscalar meson family, Phys. Rev. D **102**, no.11, 114034 (2020).
- [43] J. S. Yu, Z. F. Sun, X. Liu and Q. Zhao, Categorizing resonances  $X(1835)$ ,  $X(2120)$  and  $X(2370)$  in the pseudoscalar meson family, Phys. Rev. D **83**, 114007 (2011).
- [44] L. P. He, X. Wang and X. Liu, Towards two-body strong decay behavior of higher  $\rho$  and  $\rho_3$  mesons, Phys. Rev. D **88**, no. 3, 034008 (2013).
- [45] Z. C. Ye, X. Wang, X. Liu and Q. Zhao, The mass spectrum and strong decays of isoscalar tensor mesons, Phys. Rev. D **86**, 054025 (2012).
- [46] B. Wang, C. Q. Pang, X. Liu and T. Matsuki, Pseudotensor meson family, Phys. Rev. D **91**, no. 1, 014025 (2015).
- [47] K. Chen, C. Q. Pang, X. Liu and T. Matsuki, Light axial vector mesons, Phys. Rev. D **91**, no. 7, 074025 (2015).
- [48] D. Guo, C. Q. Pang, Z. W. Liu and X. Liu, Study of unflavored light mesons with  $J^{PC} = 2^{--}$ , Phys. Rev. D **99**, no. 5, 056001 (2019).
- [49] C. Q. Pang, J. Z. Wang, X. Liu and T. Matsuki, A systematic study of mass spectra and strong decay of strange mesons, Eur. Phys. J. C **77**, no. 12, 861 (2017).
- [50] C. Q. Pang, Y. R. Wang and C. H. Wang, Prediction for  $5^{++}$  mesons, Phys. Rev. D **99**, no. 1, 014022 (2019).
- [51] M. Ablikim *et al.* [BESIII], Future Physics Programme of BE-III, Chin. Phys. C **44**, no.4, 040001 (2020).
- [52] J. J. Dudek, R. G. Edwards, M. J. Peardon, D. G. Richards and C. E. Thomas, Toward the excited meson spectrum of dynamical QCD, Phys. Rev. D **82**, 034508 (2010).
- [53] J. J. Dudek, R. G. Edwards, B. Joo, M. J. Peardon, D. G. Richards and C. E. Thomas, Isoscalar meson spectroscopy from lattice QCD, Phys. Rev. D **83**, 111502 (2011).
- [54] C. Q. Pang, B. Wang, X. Liu and T. Matsuki, High-spin mesons below 3 GeV, Phys. Rev. D **92**, no.1, 014012 (2015).
- [55] A. M. Badalian, B. L. G. Bakker and Y. A. Simonov, Light meson radial Regge trajectories, Phys. Rev. D **66**, 034026 (2002).
- [56] F. E. Close and E. S. Swanson, Dynamics and decay of heavy-light hadrons, Phys. Rev. D **72**, 094004 (2005).
- [57] E. Eichten, K. Gottfried, T. Kinoshita, J. B. Kogut, K. D. Lane and T. M. Yan, The Spectrum of Charmonium, Phys. Rev. Lett. **34**, 369-372 (1975) [erratum: Phys. Rev. Lett. **36**, 1276 (1976)].
- [58] E. Eichten, K. Gottfried, T. Kinoshita, K. D. Lane and T. M. Yan, Charmonium: The Model, Phys. Rev. D **17**, 3090 (1978) [erratum: Phys. Rev. D **21**, 313 (1980)].
- [59] A. M. Badalian, A. V. Nefediev and Y. A. Simonov, Spin-dependent interactions in quarkonia, Phys. Rev. D **78**, 114020 (2008).
- [60] A. M. Badalian and Y. A. Simonov, Masses and decay constants of B(q) mesons in the QCD string approach, Conf. Proc. C **060726**, 1091-1094 (2006).
- [61] D. Ebert, R. N. Faustov and V. O. Galkin, Mass spectra and Regge trajectories of light mesons in the relativistic quark model, Phys. Rev. D **79**, 114029 (2009).
- [62] D. Ebert, R. N. Faustov and V. O. Galkin, Heavy-light meson spectroscopy and Regge trajectories in the relativistic quark model, Eur. Phys. J. C **66**, 197-206 (2010).
- [63] S. Godfrey and N. Isgur, Mesons in a Relativized Quark Model with Chromodynamics, Phys. Rev. D **32**, 189 (1985).
- [64] E. Laermann, F. Langhammer, I. Schmitt and P. M. Zerwas, The Interquark Potential: SU(2) Color Gauge Theory With Fermions, Phys. Lett. B **173**, 437-442 (1986).
- [65] K. D. Born, E. Laermann, N. Pirch, T. F. Walsh and P. M. Zerwas, Hadron Properties in Lattice QCD With Dynamical Fermions, Phys. Rev. D **40**, 1653-1663 (1989).
- [66] K. T. Chao, Y. B. Ding and D. H. Qin, Possible phenomenological indication for the string Coulomb term and the color

- screening effects in the quark - anti-quark potential, Commun. Theor. Phys. **18**, 321-326 (1992).
- [67] Y. B. Ding, K. T. Chao and D. H. Qin, Screened Q anti-Q potential and spectrum of heavy quarkonium, Chin. Phys. Lett. **10**, 460-463 (1993).
- [68] Y. B. Ding, K. T. Chao and D. H. Qin, Possible effects of color screening and large string tension in heavy quarkonium spectra, Phys. Rev. D **51**, 5064-5068 (1995).
- [69] B. Q. Li and K. T. Chao, Higher Charmonia and  $X, Y, Z$  states with Screened Potential, Phys. Rev. D **79**, 094004 (2009).
- [70] M. X. Duan and X. Liu, Where are  $3P$  and higher  $P$ -wave states in the charmonium family?, [arXiv:2107.14438 [hep-ph]].
- [71] Q. T. Song, D. Y. Chen, X. Liu and T. Matsuki, Higher radial and orbital excitations in the charmed meson family, Phys. Rev. D **92**, no.7, 074011 (2015).
- [72] J. Z. Wang, D. Y. Chen, X. Liu and T. Matsuki, Constructing  $J/\psi$  family with updated data of charmoniumlike  $Y$  states, Phys. Rev. D **99**, no.11, 114003 (2019).
- [73] J. Z. Wang, R. Q. Qian, X. Liu and T. Matsuki, Are the  $Y$  states around 4.6 GeV from  $e^+e^-$  annihilation higher charmonia?, Phys. Rev. D **101**, no.3, 034001 (2020).
- [74] J. Z. Wang, Z. F. Sun, X. Liu and T. Matsuki, Higher bottomonium zoo, Eur. Phys. J. C **78**, no.11, 915 (2018).
- [75] L. M. Wang, J. Z. Wang and X. Liu, Toward  $e^+e^- \rightarrow \pi^+\pi^-$  annihilation inspired by higher  $\rho$  mesonic states around 2.2 GeV, Phys. Rev. D **102**, no.3, 034037 (2020).
- [76] P. A. Zyla *et al.* [Particle Data Group], Review of Particle Physics, PTEP **2020**, no.8, 083C01 (2020).
- [77] C. Q. Pang, Excited states of  $\phi$  meson, Phys. Rev. D **99**, no.7, 074015 (2019).
- [78] A. V. Anisovich, C. A. Baker, C. J. Batty, D. V. Bugg, L. Montanet, V. A. Nikonov, A. V. Sarantsev, V. V. Sarantsev and B. S. Zou, Combined analysis of meson channels with  $I = 1$ ,  $C = -1$  from 1940 to 2410 MeV, Phys. Lett. B **542**, 8-18 (2002).
- [79] C. Hayne and N. Isgur, Beyond the Wave Function at the Origin: Some Momentum Dependent Effects in the Nonrelativistic Quark Model, Phys. Rev. D **25**, 1944 (1982).
- [80] M. Jacob and G. C. Wick, On the General Theory of Collisions for Particles with Spin, Annals Phys. **7**, 404-428 (1959).
- [81] M. Ablikim *et al.* [BESIII], Measurement of the Born cross sections for  $e^+e^- \rightarrow \eta'\pi^+\pi^-$  at center-of-mass energies between 2.00 and 3.08 GeV, Phys. Rev. D **103**, no.7, 072007 (2021).
- [82] M. Ablikim *et al.* [BESIII], Study of the process  $e^+e^- \rightarrow \phi\eta$  at center-of-mass energies between 2.00 and 3.08 GeV, Phys. Rev. D **104**, no.3, 032007 (2021).
- [83] M. Ablikim *et al.* [BESIII], Cross section measurement of  $e^+e^- \rightarrow K_S^0 K_L^0$  at  $\sqrt{s} = 2.00 - 3.08$  GeV, [arXiv:2105.13597 [hep-ex]].
- [84] M. Ablikim *et al.* [BESIII], Cross section measurements of  $e^+e^- \rightarrow K^+K^-K^+K^-$  and  $\phi K^+K^-$  at center-of-mass energies from 2.10 to 3.08 GeV, Phys. Rev. D **100**, no.3, 032009 (2019).
- [85] M. Ablikim *et al.* [BESIII], Observation of a structure in  $e^+e^- \rightarrow \phi\eta'$  at  $\sqrt{s}$  from 2.05 to 3.08 GeV, Phys. Rev. D **102**, no.1, 012008 (2020).
- [86] M. Ablikim *et al.* [BESIII], Measurement of  $e^+e^- \rightarrow K^+K^-$  cross section at  $\sqrt{s} = 2.00 - 3.08$  GeV, Phys. Rev. D **99**, no.3, 032001 (2019).
- [87] M. Ablikim *et al.* [BESIII], Observation of a Resonant Structure in  $e^+e^- \rightarrow K^+K^-\pi^0\pi^0$ , Phys. Rev. Lett. **124**, no.11, 112001 (2020).
- [88] M. Ablikim *et al.* [BESIII], Observation of a resonant structure in  $e^+e^- \rightarrow \omega\eta$  and another in  $e^+e^- \rightarrow \omega\pi^0$  at center-of-mass energies between 2.00 and 3.08 GeV, Phys. Lett. B **813**, 136059 (2021).